

## Contents lists available at ScienceDirect

# Geoderma

journal homepage: www.elsevier.com/locate/geoderma





# Tracing changes in base cation sources for Arctic tundra vegetation upon permafrost thaw

Elisabeth Mauclet <sup>a</sup>, Catherine Hirst <sup>a</sup>, Arthur Monhonval <sup>a</sup>, Emily I. Stevenson <sup>b</sup>, Merlin Gérard <sup>a</sup>, Maëlle Villani <sup>a</sup>, Hélène Dailly <sup>a</sup>, Edward A.G. Schuur <sup>c</sup>, Sophie Opfergelt <sup>a,\*</sup>

- a Earth and Life Institute, Université Catholique de Louvain, Louvain-la-Neuve, Belgium
- <sup>b</sup> Department of Earth Sciences, University of Cambridge, UK
- <sup>c</sup> Center for Ecosystem Society and Science, Northern Arizona University, Flagstaff, AZ, USA

## ARTICLE INFO

Handling Editor: Alberto Agnelli

Keywords:
Plant nutrient source
Arctic tundra
Rooting depth
Radiogenic Sr isotopes
Alaska
Eight Mile Lake

## ABSTRACT

Upon permafrost thaw, the volume of soil accessible to plant roots increases which modifies the acquisition of plant-available resources. Tundra vegetation is actively responding to the changing environment with two major directions for vegetation shift across the Arctic: the expansion of deep-rooted sedges and the widespread increase in shallow-rooted shrubs. Changes in vegetation composition, density and distribution have large implications on the Arctic warming and permafrost stability by influencing the albedo, the snow accumulation and the litter decomposition rate. A better understanding of these cumulated effects of changing vegetation on warming and permafrost requires assessing the changes in plant nutrient sources upon permafrost thaw, nutrient access being a limiting factor for the Arctic tundra vegetation development. In this study, we determined the influence of permafrost degradation on the base cation sources for plant uptake by using the radiogenic Sr isotope ratio as a tracer of source, along a permafrost thaw gradient at Eight Mile Lake in Interior Alaska (USA). As plants take up Sr from the exchangeable soil fraction with no measurable fractionation, we determined the differences in <sup>87</sup>Sr/<sup>86</sup>Sr ratio of the exchangeable Sr between shallow and deeper soil horizons, and we compared the <sup>87</sup>Sr/<sup>86</sup>Sr ratio of foliar samples for three Arctic tundra species with contrasted rooting depths (Betula nana, Vaccinium vitisidaea, and  $Eriophorum\ vaginatum)$  upon different permafrost thaw conditions. The higher foliar  $^{87}\text{Sr}/^{86}\text{Sr}$  ratios of shallow-rooted Arctic tundra shrubs (B. nana, V. vitis-idaea) was consistent with a shallow source of soil  $exchangeable \ Sr\ from\ surface\ soil\ horizons,\ whereas\ the\ lower\ foliar\ ^{87}Sr/^{86}Sr\ ratios\ of\ deep-rooted\ Arctic\ tundralled \ From\ Sr/^{86}Sr\ ratios\ of\ deep-rooted\ Arctic\ tundralled \ From\ Sr/^{86}Sr\ ratios\ of\ deep-rooted\ Arctic\ tundralled \ From\ Sr/^{86}Sr/^{86}Sr\ ratios\ of\ deep-rooted\ Arctic\ tundralled \ From\ Sr/^{86}Sr/^{86$ sedges (E. vaginatum) reflected a source of Sr from deeper soil horizons. There is a shift between poorly and highly thawed soil profiles towards lower foliar <sup>87</sup>Sr/<sup>86</sup>Sr ratios in both deep- and shallow-rooted plant species. This shift supports that micro-landscape variability in the exchangeable base cation reserve with soil depth represents a key source of readily available nutrients for both shallow- and deep-rooted plant species upon permafrost thaw. This study highlights a key change in plant nutrient source to consider upon thaw. This finding lies beyond the common view that nutrient release at the permafrost thaw front preferentially benefits deeprooted plant species.

## 1. Introduction

In recent decades, Arctic and sub-Arctic regions have warmed and experienced rapid changes (Post et al., 2019). Increasing air temperature has led to important permafrost degradation, with active layer thickening, ground subsidence, changes in hydrology, and shifts in vegetation (Jorgenson et al., 2006; Lloyd et al., 2003; Schuur and Mack, 2018; Yang et al., 2010). Ongoing permafrost degradation and active layer

thickening enlarge boundaries of plant-available soil volumes, thereby modifying the ecosystem equilibrium and resource acquisition. Moreover, changes in soil hydrology also influence soil mineral element distribution and soil–plant nutrient cycling (Hirst et al., 2022; Koch et al., 2013; Tetzlaff et al., 2015; Walvoord and Kurylyk, 2016).

Arctic tundra vegetation is mainly composed of vascular plant functional types such as graminoids, forbs, deciduous and evergreen shrubs, and non-vascular species such as mosses and lichens (Walker

E-mail address: sophie.opfergelt@uclouvain.be (S. Opfergelt).

https://doi.org/10.1016/j.geoderma.2022.116277

<sup>\*</sup> Corresponding author.

et al., 2005). Upon warming, the tundra vegetation is responding to changing environments through shifts in the composition, density and distribution of plant communitites, thereby causing several opposing feedbacks on Arctic warming that remain poorly understood throughout the Arctic (Pearson et al., 2013). Among others, ongoing changes in vegetation biomass composition have massive feedbacks on climate because plant species directly influence solar radiation and soil surface shading, snow trap and soil insulation, litter decomposition rate and nutrient cycling (Chapin et al., 2005; Sturm et al., 2001a). In nutrientlimited permafrost soils, Arctic tundra plant strategies for nutrient acquisition and their response to changing environment may largely influence the shifts in tundra vegetation upon warming. In recent decades, the shallow-rooted shrubs have expanded across northern latitude ecosystems (Jonsdottir et al., 2005; Shaver et al., 2001; Sturm et al., 2001b), whereas deep-rooted sedges (as part of the graminoids) have dominated permafrost areas with wetter soil conditions (Jorgenson et al., 2015; Jorgenson et al., 2001; van der Kolk et al., 2016). These two typical Arctic tundra plant functional types rely on different rooting system strategies (Iversen et al., 2015). Shrubs (such as B. nana and V. vitis-idaea) initiate their root growth earlier than sedges, and take advantage of the nutrient pulse after snowmelt, in the early growing season (Wang et al., 2016). The deep roots of sedges (such as E. vaginatum) access deeper nutrient pools, and benefit first from the release of the newly thawed nutrients upon increasing permafrost thaw (Blume-Werry et al., 2019; Hewitt et al., 2018; Keuper et al., 2017). To better constrain the influence of rooting system vertical distribution (i. e., vertical nutrient access) on competitiveness traits of Arctic plant species and further shift in vegetation, there is a need to identify the changes in nutrient sources for Arctic tundra vegetation upon permafrost thaw.

Plants take up base cations (Ca, K, Mg) as nutrients from the exchangeable soil fraction, and Sr is a chemical analog to Ca (Drouet et al., 2007) which is a key macronutrient together with K and Mg (DalCorso et al., 2014). Plants take up Sr together with Ca (Åberg et al., 1989; Capo et al., 1998; Graustein and Armstrong, 1983; Poszwa et al., 2004). Strontium has four natural stable isotopes:  $^{88}$ Sr (natural abundance of 82.58 %),  $^{87}$ Sr (7.0 %),  $^{86}$ Sr (9.86 %) and  $^{84}$ Sr (0.56 %). Only <sup>87</sup>Sr is "radiogenic" and results from the radioactive β–decay of <sup>87</sup>Rb (with a half-life of about 49 billion years). The isotope ratio <sup>87</sup>Sr/<sup>86</sup>Sr is largely used to trace cation origin at the Earth surface as a function of geological processes involving bedrock lithology and mineral weathering (Drouet et al., 2007; Hajj et al., 2017; Wang and Tang, 2020). As there is no measurable fractionation of radiogenic Sr isotopes during biological processes, the <sup>87</sup>Sr/<sup>86</sup>Sr ratio in plant tissues directly reflects source materials and are particularly useful for nutrient provenance studies (Blum et al., 2000; Chadwick et al., 1999; Kennedy et al., 1998; Reynolds et al., 2012; Vitousek et al., 1999).

This study was carried out with the objective to determine the influence of permafrost thaw on the base cation sources for plant uptake. More specifically, we use the radiogenic Sr isotopes as a tracer of source for plant base cation uptake along a permafrost thaw gradient at Eight Mile Lake, Interior Alaska, USA. We determined the differences in  $^{87}\text{Sr}/^{86}\text{Sr}$  ratio of the exchangeable Sr between shallow and deeper soil horizons, and we compared the  $^{87}\text{Sr}/^{86}\text{Sr}$  ratio of foliar samples for three Arctic tundra species with contrasted rooting depths (*B. nana, V. vitisidaea*, and *E. vaginatum*) upon soil profiles with different active layer thickness (poorly thawed and highly thawed soil profiles).

## 2. Environmental setting

The study was conducted at the Eight Mile Lake (EML) research site in Healy, Interior Alaska, USA ( $63^{\circ}52'42$  N,  $149^{\circ}15'12$  W). The site is underlain by degrading permafrost in the discontinuous permafrost zone (Natali et al., 2011; Osterkamp et al., 2009). Climate is characterized by mean monthly air temperature ranging from -16 °C in December to + 15 °C in July, mean annual air temperature of -0.94 °C and average

annual precipitation of 381 mm (2007–2017) (Healy and McKinley Stations, Western Regional Climate Center, and National Oceanic and Atmospheric Administration National Centers for Environmental Information [NOAA]). Soils are classified as Histic Turbic Cryosols (IUSS Working Group WRB, 2015), characterized by a 35 to 55 cm thick organic layer (>20 % of organic C content) at the surface, lying above a cryoturbated mineral soil horizon (5–20 % of organic C) formed from glacial till and loess (Hicks Pries et al., 2012; Osterkamp et al., 2009; Vogel et al., 2009).

Within the EML watershed, a natural gradient in permafrost thaw and thermokarst formation has developed since the mid to late 1980 s (Schuur et al., 2007), and has been defined as the Gradient site. The site is located on a gentle (<5°) north-facing slope (Osterkamp and Romanovsky, 1999; Schuur et al., 2007) and has been monitored since 1990 to follow the impact of permafrost degradation on ground subsidence, thaw depth and water table depth (Schuur et al., 2009). Mean annual soil temperature at 10 cm depth at the site is 0.72  $\pm$  0.66  $^{\circ}\text{C}$ (2004-2018; Schuur et al., 2021), with negative soil temperature at 10 cm depth during the winter season (-3.54  $\pm$  1.72  $^{\circ}\text{C}$  during the nongrowing season relative to 5.61  $\pm$  0.94  $^{\circ}$ C during the growing season). The soil temperature at the end of the growing season is 4.76  $\pm$  0.76  $^{\circ}$ C at 10 cm and  $1.94 \pm 0.19$  °C at 40 cm (1–15 September 2019; Celis et al., 2019). Field measurements in late August 2019 reported contrasted maximum active layer thicknesses (ALT; from 40 to 90 cm) and water table depths (from 0 to 40 cm) across the site. Based on the modern active layer defined at  $\sim$  60 cm at the center of the site (Hutchings et al., 2019), we distinguish "poorly" (ALT  $\leq$  60 cm) and "highly" (ALT > 60 cm) thawed permafrost sites (Table A.1). The study site is located on moist acidic tundra (pH<sub>soil</sub> ~ 3 to 5; Bracho et al., 2016; Osterkamp et al., 2009), with a dominance of tussock-forming sedges, such as Eriophorum vaginatum L. and Carex bigelowii Torr. ex Schwein, evergreen shrubs (e.g., Andromeda polifolia L., Rhododendron tomentosum Harmaja, Vaccinium vitis-idaea L., and Empetrum nigrum L.), deciduous shrubs (e.g., Vaccinium uliginosum L. and Betula nana L.), and forbs (e.g., Rubus chamaemorus L.). Non-vascular plant cover is dominated by mosses (mainly Sphagnum spp., Dicranum spp., and feather mosses including Hylocomium splendens and Pleurozium schreberi,) and lichen species (e.g., Nephroma spp., Cladonia spp., and Flavocetraria cucullata) (Deane-Coe et al., 2015; Natali et al., 2012; Schuur et al., 2007). The thermokarst development at EML has initiated a shift in the vegetation cover, with evergreen and deciduous shrubs (as B. nana), and forbs becoming dominant at the expense of tussock forming sedges (as E. vaginatum) (Jasinski et al., 2018; Schuur et al., 2007).

## 3. Materials and methods

## 3.1. Sampling method

A field campaign took place at the Gradient site (EML) between the end of August and mid-September 2019 (i.e., at the late season period) to collect soil profiles with contrasts in ALT (measured with a metal probe; Table A.1) and the associated vegetation.

In total, seven soil cores were collected to cover contrast in permafrost thaw: four poorly thawed soil profiles with ALT  $\leq 60$  cm (Min1, Min3, Mod1, Ext1), and three highly thawed soil profiles with ALT > 60 cm (Mod2, Mod3, Ext3) (Fig. 1). Soils were sampled to a maximum depth of 120 cm and subdivided into 5 cm to 10 cm layers. Active layer samples were collected using a hammer and chisel as deep as possible (up to 45 cm, unless water table was higher than 45 cm). Below 45 cm depth, active layer and permafrost samples were collected using a steel pipe (diameter 4.5 cm) that was manually hammered into the soil using a sledgehammer (Palmtag et al., 2015). The sampling procedure likely induces compaction in the active layer, while compaction in frozen soil can be considered negligible. In the lab, soil samples (n = 85) were dried at air temperature in a ventilated and temperature-controlled room and sieved through a 2 mm sieve.

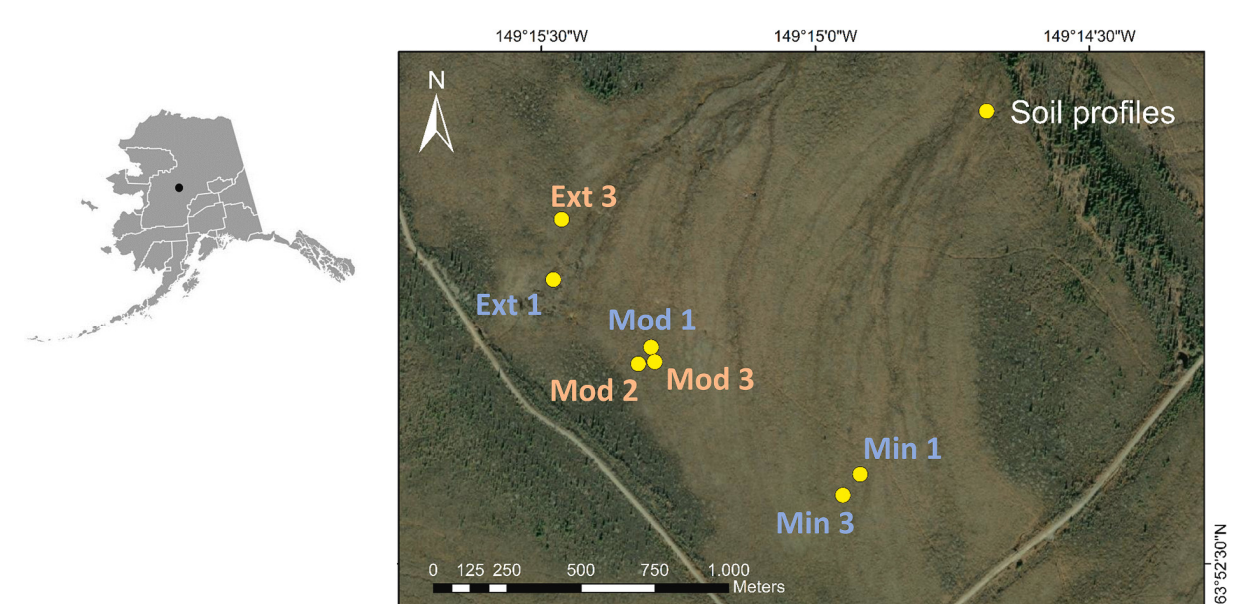


Fig. 1. Location of the sampling sites in Eight Mile Lake, Alaska, USA with the poorly thawed (blue label) and the highly thawed (orange label) soil profiles. Source for the base map: Esri, DigitalGlobe, GeoEye, Earthstar Geographics, CNES/Airbus DS, USDA, USGS, AeroGRID, IGN, and the GIS User Community. (Figure in color).

For the vegetation, we selected three of the most abundant vascular species of the site (Jasinski et al., 2022; Mauclet et al., 2022a; Natali et al., 2011; Schuur et al., 2007; Villani et al., 2022): *E. vaginatum* (sedges, n=7), *B. nana* (deciduous shrubs, n=7), and *V. vitis-idaea* (evergreen shrubs, n=7). The maximum rooting depths reported for these species at the study site are  $\sim$ 30–40 cm for *E. vaginatum*,  $\sim$ 20–35 cm for *B. nana*, and 20–40 cm for *V. vitis-idaea* (Hewitt et al., 2018), with deeper mean maximum rooting depths for the three studied plant species in sedge-dominated tundra (<25 % cover as shrubs) than in shrubdominated tundra (25–75 % cover as shrubs). We sampled fully formed leaves over an area of  $\sim$ 5 m² around each of the seven soil cores. We also collected tissues of the lichen *Flavocetraria cucullata* as a bulk composite sample across the different core sites (composite sample, n=1). Leaf samples were dried at 60 °C and shredded.

## 3.2. Characterization of the total soil fraction

The soil  $pH_{H2O}$  was measured on all soil samples (n = 85) with the pH-meter (Mettier Toledo SevenCompact DuoS213) connected to the pH probe (Inlab micro) (data in Table A.2). Mineral soil samples were mixed with  $H_2O$  in a 1:5 ratio (Peech, 1965), whereas organic soil samples required adaptation of the solid:solution ratio (1:15) to allow the measurement with the pH probe due to the high water retention capacity of the organic matter. The pH probe was calibrated for pH 4 and 7 before measurement.

The total soil carbon content was determined on all soil samples (n = 85) with the C, N, S elemental analyzer vario EL CUBE (ELEMENTAR ®, Germany). Each sample was measured twice and the average standard deviation for the total soil carbon content was ~5 %, with the detection limit <0.1 %. As the presence of carbonate minerals was not detected by X-ray diffraction (Fig. A.1), the total soil carbon content is considered equivalent to the soil organic carbon (SOC) content. The C measurements on soil samples (n = 85; 7 profiles at the Gradient site in 2019) are reported to the dry soil matrix (105 °C) (data in Table A.2). These analyses were used to distinguish organic horizons (SOC > 20 %) and mineral horizons (SOC  $\leq$  20 %) (Hicks Pries et al., 2012).

The total concentrations in Ca, K, Mg, and Na in bulk soils were determined for three soil profiles selected to cover poorly and highly thawed permafrost soils (n=38; Min1, Mod3, Ext3; data in Table A.2) by inductively coupled plasma optical emission spectroscopy (ICP-OES,

iCAP 6500 ThermoFisher Scientific, Waltham, USA) after alkaline fusion. Briefly, a portion of the soil sample finely ground in a mortar was mixed with lithium metaborate and lithium tetraborate, and heated up to 1000 °C. The fusion bead was dissolved in 2.2 N HNO3 at 80 °C and stirred until complete dissolution (Chao and Sanzolone, 1992). The loss on ignition was assessed at 1000 °C and total element content was expressed in reference to the dry weight at 105 °C. The accuracy of mineral element (Ca, K, Mg, and Na) analyses was assessed using trueness ( $\pm 2\%$ ,  $\pm 5$  %,  $\pm 2$  %, and  $\pm 2$  %; respectively) on the USGS basalt reference material BHVO-2 (Wilson and Labay, 1997) and the analytical precision ( $\pm 0.5$  %) for each element. The accuracy of ICP-OES measurements was also validated by repeated measurements on the lichen reference material IAEA-336 (Mauclet et al., 2022a), and on two soil reference materials (GBW07401 (GSS-1); GBW07404 (GSS-4); Monhonval et al., 2021). The limits of detection (LOD) were 0.05 mg  $L^{-1}$  $0.01 \text{ mg L}^{-1}$ ,  $0.001 \text{ mg L}^{-1}$ , and  $0.02 \text{ mg L}^{-1}$  for Ca, K, Mg, and Na, respectively. The blank levels were below the detection limit for Ca, K, Mg, Na. We used the total reserve in bases (TRB expressed in  $cmol_c kg^{-1}$ ) Herbillon, 1986) as a weathering index, which corresponds to the sum of total Ca, K, Mg, and Na concentrations.

We assessed by X-ray diffraction the mineralogy of 21 bulk soil samples selected from five soil profiles to cover poorly and highly thawed permafrost soil profiles (Min3, Mod2, Mod3, Ext2, Ext3). The mineralogy of bulk samples was determined on powder finely ground in a mortar using a Bruker D8 Advance diffractometer (Cu K $\alpha$ , 40 kV, 30 mA, primary Soller slit 2°, divergence slit 1 mm, secondary Soller slit 2°, anti-scattering slit 1 mm, detector slit 0.2 mm, registration range (2 $\theta$ ): 2 to 90° at 1°/min, detection limit of 5 %).

## 3.3. Characterization of total and exchangeable Sr in soils

The total Sr concentration was determined in all soil samples (n = 85) using a non-destructive portable X-ray fluorescence (pXRF) device Niton xl3t Goldd+ (Thermo Fisher Scientific, Waltham, USA). The pXRF analyses were conducted in laboratory conditions, using a lead stand to protect the operator from X-rays emission (data in Table A.3). For the measurement, the dried sample powder was placed on a circular plastic cap (2.5 diameter) provided with a transparent thin film (prolene 4  $\mu$ m) at its base, in order to reach  $\sim 1$  cm of sample thickness. Each sample was scanned for a total measurement time of 90 s. When the LOD was

reached for the pXRF device (95 mg kg $^{-1}$  for Sr), the value was set to 0.5-times the minimal concentration measured within the entire set of data, which is an arbitrary number but conventionally used for data statistical treatment (Reimann et al., 2008). The precision of the pXRF method is  $\sim$ 4 % for Sr concentration in soil based on 5 repetitions on 31 samples representative of the organic and mineral layers (i.e., standard deviation divided by the mean, expressed in % to the mean). The pXRF-measured concentrations were calibrated with another accurate wet chemistry method (Monhonval et al., 2021) using measurements by inductively coupled plasma optical emission spectroscopy (ICP-OES; iCAP 6500, Thermo Fisher Scientific, Waltham, USA) after alkaline fusion on soil samples from the site (n = 38; section 3.2).

The fraction of exchangeable Sr was extracted from all soil samples (n = 85) using 1 M NH<sub>4</sub>Ac (method adapted from (Metson, 1956). The concentration in exchangeable Sr within the extracts was measured by ICP-OES (data in Table A.3). The accuracy on the Sr analyses was assessed using trueness ( $\pm 6\%$ ) on the USGS basalt reference material BHVO-2 (Wilson and Labay, 1997) and the analytical precision ( $\pm 0.5\%$ ). The limit of detection (LOD) was 0.0001 mg L<sup>-1</sup> and the blank level was below detection limit for Sr.

## 3.4. Measurement of radiogenic Sr isotopic composition

The radiogenic Sr isotope composition was measured on the exchangeable Sr fractions in each soil layers (n=85; Table A.3) and the corresponding foliar samples (n=22; Table A.4) of three plant species of the standing vegetation for the seven soil profiles (Min1, Min3, Mod1, Ext1, Mod2, Mod3, Ext3).

Samples were prepared in a clean laboratory (class 100, laminar flow). The vegetation samples were mineralized at 450 °C and dissolved in sealed Teflon vials with HF/HNO3. For the exchangeable soil fractions, the dissolved organic carbon was removed from the extracts by reflux with concentrated HNO3 and  $\rm H_2O_2$  in sealed Teflon vials on a hot plate (180 °C). Solutions from digested vegetation and exchangeable Sr were evaporated to dryness and redissolved in 2 % HNO3. The Sr concentration in the resulting solutions was measured by ICP-OES. An aliquot of 500 ng of Sr was dried down and picked up in 100  $\mu l$  of 3 M HNO3. To purify Sr, the sample was loaded onto Biorad microspin column containing 500  $\mu l$  of pre-cleaned Strontium specific resin (50–100  $\mu m$  Triskem), and eluted in several stages with HNO3 (Aciego et al., 2009). The total procedural Sr blank is <0.1 % of the total Sr analyzed for a typical Sr analysis.

Strontium isotope measurements were carried out by MC-ICP-MS (Neptune Plus<sup>TM</sup> High Resolution Multicollector ICP-MS, Thermo Fisher Scientific, Earth & Life Institute, UCLouvain, Belgium) in wet plasma mode using a PFA nebulizer of 100 µl.min<sup>-1</sup> uptake rate. The analyses were performed in 2 % HNO3 matrix, with a typical sensitivity of 7 V for 100 ppb Sr. Each sample was measured three times and the results are expressed as 87Sr/86Sr ratio. According to the relative enrichment in <sup>87</sup>Sr (radiogenic Sr), the higher <sup>87</sup>Sr/<sup>86</sup>Sr ratios are termed "more radiogenic" and the lower 87Sr/86Sr ratio termed "less radiogenic". External precision on the in-house standard Sr ICP solution was 0.708631  $\pm$  0.000012 (2SD, n = 107). The reference material SRM987 was used to assess the precision of column chemistry and the analytical procedure and yielded a value of 0.710274  $\pm$  0.000046 (2SD, n=148) consistent with previous studies (e.g., 0.710264  $\pm$  0.000016; Stevenson et al., 2016) and within error with the certified value of the NIST SRM987 (0.071034  $\pm$  0.00026). We can be confident that the NH<sub>4</sub>Ac matrix does not induce bias on Sr isotopic measurements according to the measured <sup>87</sup>Sr/<sup>86</sup>Sr ratios on the reference material SRM987 mixed with 1 M NH<sub>4</sub>Ac and purified similarly to other samples (0.710263  $\pm$  0.000002, 2SD, n = 2), i.e., similar to published values (0.710264  $\pm$  0.000016; Stevenson et al., 2016). To assess statistical differences between two datasets, we performed the Wilcoxon test using R software version R.3.6.1 (R Core Team, 2019).

#### 4. Results and discussion

4.1. Distribution of the exchangeable radiogenic Sr isotopic composition in Arctic tundra soils

The exchangeable Sr pool represents between  $\sim\!2$  to 70 % of the total Sr concentration (Table A.3), with the highest proportions in the upper soil layer (concentrations in exchangeable Sr varying from 2.8 to 19.3 mg kg\_{soil}^{-1}, Table A.3). The exchangeable Sr soil fraction is characterized by  $^{87}$ Sr/ $^{86}$ Sr ratios ranging between 0.7083 and 0.7135 (Fig. 2a, Table A.3), with the highest values in the soil surface horizons.

The higher  $^{87}$ Sr/ $^{86}$ Sr ratios (more radiogenic) of the exchangeable Sr in surface soil horizons than in deeper soil horizons (mean surface horizons = 0.7105  $\pm$  0.0010; mean deep horizons = 0.7089  $\pm$  0.0003; Wilcoxon test p-value < 0.01) can be explained by differences in soil mineralogy between surface and deeper horizons (Fig. A.1). The soil mineralogy is characterized by the presence of clay minerals (most likely vermiculite, kaolinite, illite), mica (muscovite), and quartz in the upper part of the soil profiles, and more primary minerals (plagioclase, K-feldspar, amphibole, quartz, muscovite) with the clay minerals (most likely vermiculite, kaolinite, illite) in deeper horizons. This difference in soil mineralogy with depth provides a higher proportion in more radiogenic (K-rich) minerals in the upper part of the soil profile and a higher proportion of less radiogenic (Ca-rich) minerals in deeper soil horizons (Bataille et al., 2020; Drouet et al., 2007; Hajj et al., 2017; Pett-Ridge et al., 2009; Wang and Tang, 2020).

Mineral weathering is the main source of exchangeable Sr in soils (Bullen and Chadwick, 2016; Chadwick et al., 2009; Drouet et al., 2005; Keller et al., 2007). As more easily weathered minerals (e.g., plagioclase: Goldich, 1938) have lower <sup>87</sup>Sr/<sup>86</sup>Sr ratios than less easily weathered Kfeldspars and clay minerals (such as illite) (Bataille et al., 2020; Capo et al., 1998; Wang and Tang, 2020), the exchangeable Sr released upon mineral weathering is expected to be less radiogenic in deeper horizons containing plagioclase. The higher proportion of primary minerals in deeper soil horizons is reflected using the total reserve in bases (TRB) as a chemical weathering index (decreasing TRB with increasing weathering). Among the seven soil profiles, the deeper mineral horizons present higher TRB values than the organic surface horizons (deep horizons =  $188 \pm 14 \text{ cmol}_c \text{ kg}^{-1}$ ; surface horizons =  $43 \pm 10 \text{ cmol}_c \text{ kg}^{-1}$ ; Wilcoxon test p-value < 0.01; Table A.2), supporting a higher proportion of primary minerals at depth (i.e., a lower weathering degree). The negative relationship between soil TRB and exchangeable <sup>87</sup>Sr/<sup>86</sup>Sr ratios  $(R^2 = 0.67; Fig. 2b)$  supports the dominant contribution of primary mineral dissolution to exchangeable Sr in deeper horizons, and a contribution from clay mineral dissolution in organic surface horizons. This hypothesis of clay mineral dissolution is supported by the negative correlation between soil pH and the exchangeable <sup>87</sup>Sr/<sup>86</sup>Sr ratios (R<sup>2</sup> = 0.32; Fig. 2c). The acidic conditions in organic surface soil horizons (soil pH < 4.1; Table A.2) can favor clay dissolution (e.g., Cornelis et al., 2010).

Atmospheric deposition of aerosols and dust may contribute to enrich surface soil horizons with exogenous inorganic rock-derived elements such as Sr, therefore modifying the radiognenic Sr isopotic signature in surface (Derry and Chadwick, 2007; Graustein and Armstrong, 1983; Vitousek et al., 1999). Specifically, Sr derived from marine aerosols is considered as an important source of biologically-available Sr in some highly weathered and/or coastal ecosystems (Chadwick et al., 2009; Graustein and Armstrong, 1983; Pearce et al., 2015). However, the influence of marine deposition is negligible in the continental environment of Interior Alaska (Hirst et al., 2022), and the potential atmospheric Sr input would represent a limited amount of Sr compared to the Sr amount in the 12 000 years old loess accumulated and serving as parent material for these soils (Hutchings et al., 2019). Consequently, the influence of atmospheric input on the radiogenic Sr isotopic signature of exchangeable Sr fraction at EML is likely limited.

One observation is that the range of exchangeable  $^{87}\mathrm{Sr}/^{86}\mathrm{Sr}$  ratios is

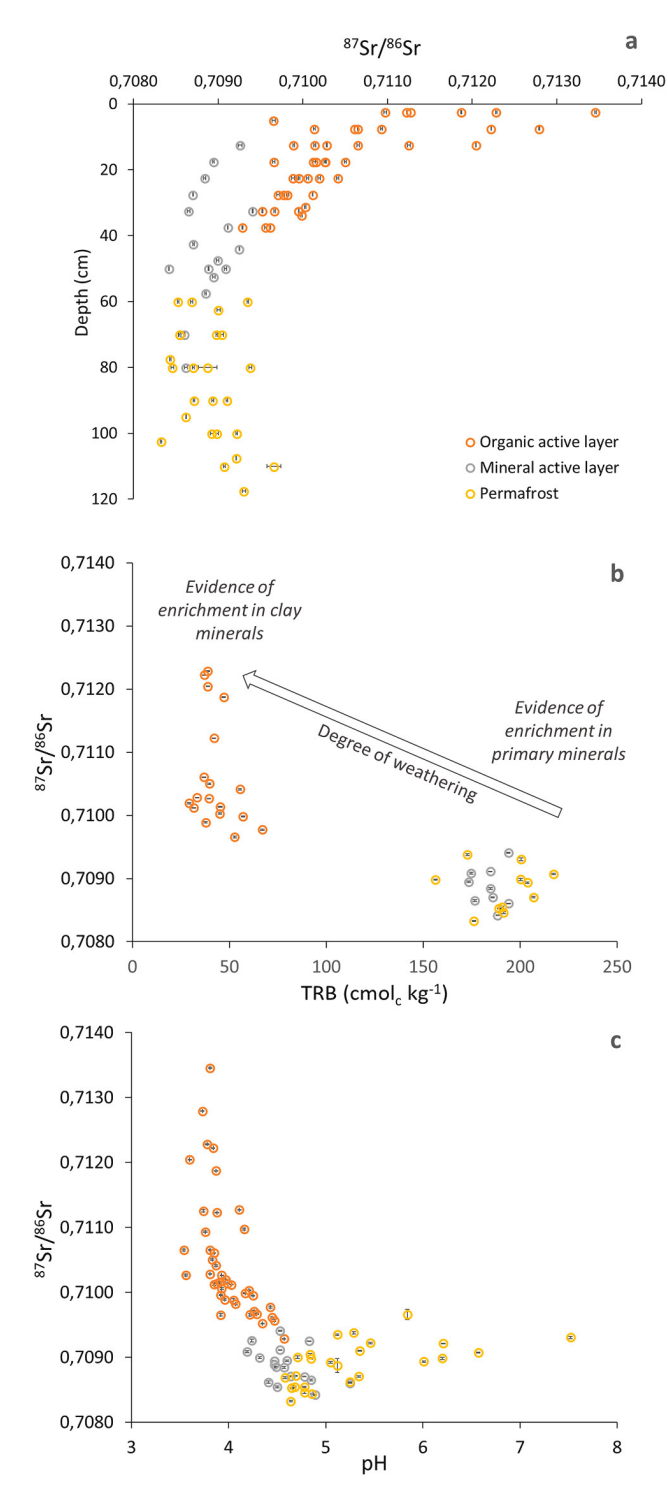


**Fig. 2.** Distribution of  ${}^{87}\text{Sr}/{}^{86}\text{Sr}$  ratios in the exchangeable Sr soil fractions for the seven studied permafrost soil profiles at the Gradient site (Eight Mile Lake, Interior Alaska, USA): (a) with depth (n = 85); (b) with the total reserve in bases (TRB, Herbillon, 1986) (n = 38, data available for three soil profiles); (c) with soil pH (n = 85). Error bars for isotopic measurements are smaller than the data points. (**Figure in color**).

narrower (between 0.7083 and 0.7101) for soil horizons below the water table than for soil horizons above water table (between 0.7096 and 0.7135) (Fig. 3 for all soil profiles; Fig. A.2 for individual soil profiles). These data suggest the transport of dissolved Sr by the fluctuating water table in water-saturated soil layers (i.e., organic and mineral soil horizons below the water table). In Arctic tundra ecosystems, water

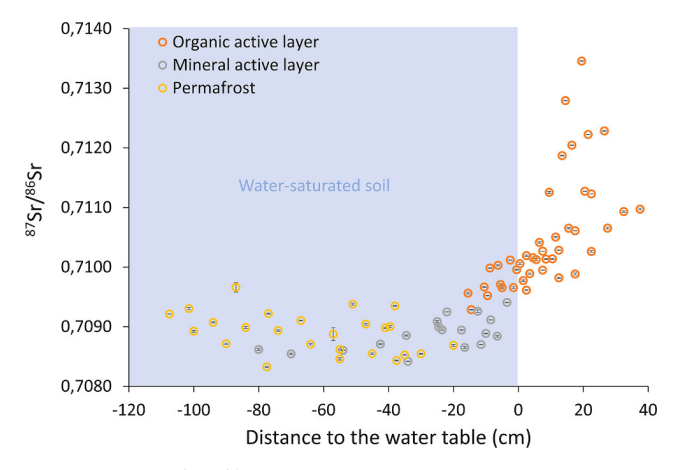


**Fig. 3.** Evolution of  $^{87}$ Sr, $^{86}$ Sr ratios of the exchangeable soil fraction according to the distance to the water table for the seven soil profiles studied (n = 85) at the Gradient site (Eight Mile Lake, Interior Alaska, USA). Error bars for isotopic measurements are smaller than the data points. (**Figure in color**).

drainage can be limited by the presence of permafrost (Kwon et al., 2019; Lewis et al., 2012; Yoshikawa and Hinzman, 2003) and the dynamic evolution of water table depth may influence the distribution of soluble cations (such as Sr) along the soil profile. This can explain a similar range of radiogenic Sr ratios of the exchangeable fraction dominated by a contribution from the dissolution of primary minerals in water-saturated soil layers. In contrast, surface horizons are generally unsaturated soil layers (i.e., organic soil horizons above the water table) not affected by the water transport of soluble element. One soil profile (Mod2) presents water-saturated surface horizons. According to our hypothesis, the surface horizons of that profile present a less pronounced contrast in exchangeable radiogenic Sr isotopic signature between surface and deep soil horizons (from 0.7097 in surface to 0.7085 at depth; Fig. A.2d) than the other soil profiles. These data support that in Mod2 profile, water transport of soluble Sr over the entire soil profile has led to the contribution of (less radiogenic) Sr from deeper soil horizons to surface horizons.

# 4.2. Radiogenic Sr isotopes to trace specific-plant base cation sources

Foliar tissues of the three studied vascular plant species show contrasted  $^{87}$ Sr/ $^{86}$ Sr ratios (Wilcoxon test *p*-value < 0.01; as illustrated in Fig. 4 and Fig. A.2), with the lowest values in E. vaginatum (mean  $^{87}\text{Sr}/^{86}\text{Sr} = 0.7096 \, \pm \, 0.0003, \; n = 7),$  followed by B. nana (mean  $^{87} \text{Sr}/^{86} \text{Sr} = 0.7105 \pm 0.0003, \, n = 7)\text{, and the highest values in V. vitis-}$ idaea (mean  $^{87}\text{Sr}/^{86}\text{Sr} = 0.7113 \pm 0.0004, \, n = 7$ ) (Table A.4). As foliar isotopic signature in radiogenic Sr directly reflects the plant nutrient sources (i.e., the exchangeable soil fraction; (Chadwick et al., 2009; Kennedy et al., 1998; Vitousek, 2004), our data support that the three plant species take up their base cations from different sources. Along soil profiles, the decreasing values of <sup>87</sup>Sr/<sup>86</sup>Sr ratios in the exchangeable Sr fraction with depth (described in section 4.1) represent base cation pools with different radiogenic Sr isotopic signatures. With increasing soil depth, there is an increase in the available exchangeable base cations, as shown by the significant increase in base saturation with depth between organic active layer and mineral active layer (Wilcoxon test p-value < 0.01; base saturation representing the proportion of the soil exchange capacity occupied by the exchangeable base cations Ca, K, Mg, Na; Fig. 5c). The difference in foliar <sup>87</sup>Sr/<sup>86</sup>Sr composition between plant species supports that even if a similar range of maximum rooting depths is reported at the site for the three studied plant species ( $\sim$ 30-40 cm for E. vaginatum, ~20-35 cm for B. nana, and 20-40 cm for V. vitis-idaea; Hewitt et al., 2018; Fig. 5a), the three plant species target different sources of base cations from the organic and mineral horizons of the

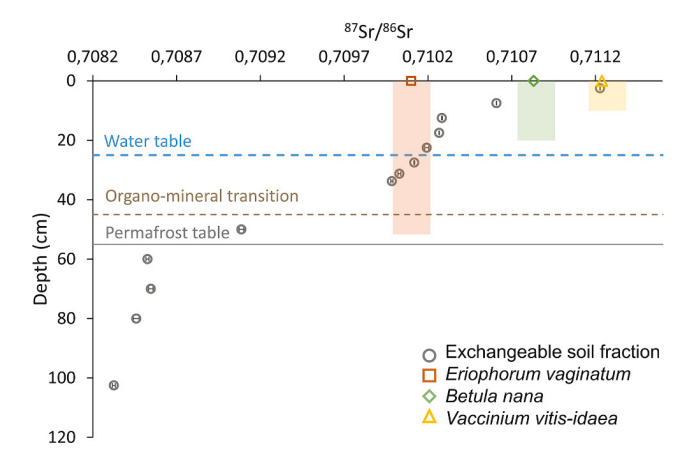


Fig. 4. Distribution of the  ${}^{87}$ Sr/ ${}^{86}$ Sr ratios of exchangeable soil fraction with depth for a poorly thawed permafrost soil profile (Min1; n = 13) at the Gradient site (Eight Mile Lake, Interior Alaska, USA). Specific foliar  ${}^{87}$ Sr/ ${}^{86}$ Sr ratios of three typical Arctic tundra plant species (*E. vaginatum*, *B. nana* and *V. vitis idaea*) lying above the soil profile are presented at the surface. The colored boxes stand for the fictive soil areas of root exploration for each plant species (Iversen et al., 2015). Error bars for isotopic measurements are smaller than the data points. The full grey line indicates the permafrost table, the brown dotted line is for the transition between organic (SOC > 20%) and mineral (SOC  $\le$  20%) soil layers, and the blue dotted line is for the water table. (Figure in color).

active layer. High foliar <sup>87</sup>Sr/<sup>86</sup>Sr ratios in shrubs (*B. nana*, *V. vitis-idaea*) reflect a shallow nutrient uptake from more radiogenic exchangeable Sr in soil surface in the organic active layer (Fig. 4). In contrast, the lower foliar <sup>87</sup>Sr/<sup>86</sup>Sr ratios in the sedge *E. vaginatum* reflect ratios from deeper sources of exchangeable Sr from the mineral active layer (Fig. 4).

For two soil profiles (Mod1 and Mod2), the foliar <sup>87</sup>Sr/<sup>86</sup>Sr ratios in the shrub V. vitis-idaea (and B. nana to a lower extent) exceed the range of exchangeable <sup>87</sup>Sr/<sup>86</sup>Sr ratios measured in the corresponding soil profile (Fig. A.2b-d). We raise two hypotheses to explain these observations. Firstly, leaf longevity of the evergreen shrub V. vitis-idaea expands over several growing seasons (Karlsson, 1985). Therefore, foliar tissues accumulate nutrients immobile in the leaf (such as Sr) and may integrate the radiogenic Sr isotopic signature of exchangeable soil fraction from previous growing seasons. Considering the deepening of the active layer over the growing season and the seasonal variability of the active layer thickness (Schuur et al., 2021), the foliar Sr isotopic integrates variable base cation sources over time. This may contribute to explain the difference in <sup>87</sup>Sr/<sup>86</sup>Sr ratios between the evergreen shrub foliar tissues and the seasonal source of exchangeable Sr. Conversely, we expect the annual foliar cycling of deciduous plant species (here, E. vaginatum and B. nana) to be more responsive to changes in radiogenic Sr isotopic signature of the exchangeable soil fraction. As a result, <sup>87</sup>Sr/<sup>86</sup>Sr ratios in deciduous foliar tissues are more likely to reflect the seasonal radiogenic Sr isotopic signature of exchangeable soil fraction. Secondly, the contribution of atmospheric deposition of Sr is expected to be limited, but could have locally brought exogenous Sr and potentially modified the site-specific isotopic foliar signature in radiogenic Sr (Probst et al., 2000). We tested this hypothesis by measuring the radiogenic Sr isotopic signature of the lichen Flavocetraria cucullata, which is a widespread lichen species across the Arctic tundra ecosystems known as a bioindicator of atmospheric composition (Anderson et al., 2022; Naeth and Wilkinson, 2008). The higher 87Sr/86Sr ratio in the lichen composite sample (0.7133  $\pm$  0.0001, n = 1, Table A.4) than in the foliar samples of V. vitis-idaea (mean  $= 0.7113 \pm 0.0004$ , n = 7) supports that if Sr derived from atmospheric deposition accumulates locally, this would lead to a more radiogenic contribution than Sr derived from soil minerals. This would therefore contribute to increase the exchangeable <sup>87</sup>Sr/<sup>86</sup>Sr ratios within the top surface soil horizons. If present, exogenous inputs of Sr are more likely to influence the foliar radiogenic Sr signature of shallow-rooted shrubs as *V. vitis-idaea* (Fig. A.2b-d) than deep-rooted species.

## 4.3. Potential influence of thawing permafrost on plant base cation uptake

In order to assess the influence of permafrost thaw on the base cation source for vegetation, we distinguish the foliar signatures in radiogenic Sr between plant species from poorly (ALT  $\leq 60$  cm) and highly (ALT > 60 cm) thawed permafrost soil profiles. Interestingly, for the three plant species studied, we observe a shift towards a range of lower foliar  $^{87}\text{Sr}/^{86}\text{Sr}$  ratios on highly thawed relative to poorly thawed permafrost soil profiles (Fig. 6). We investigate here whether this shift can be explained by the rooting systems accessing deeper and less radiogenic sources of Sr in highly thawed relative to poorly thawed permafrost soil profiles.

To determine the mass fraction of Sr assimilated by the sedge and shrub species between the "soil surface" and the "deeper soil horizons", we used a radiogenic Sr isotope mass balance on foliar samples with the Eq. (1):

87Sr/86Sr foliar = 
$$(87Sr/86Sr surface horizons \times f) + (87Sr/86Sr deep horizons \times (1 - f))$$
 (1)

With f standing for the fraction of exchangeable Sr taken up by plant in soil surface horizons (f is comprised between 0 and 1), the  $^{87}$ Sr $_{\rm surface}$  horizons ratio corresponding to the isotopic ratio of exchangeable Sr averaged for the soil "surface horizons", and the  $^{87}$ Sr $_{\rm surface}$  horizons ratio corresponding to the isotopic ratio of exchangeable Sr averaged for the "deep horizons".

To cover the full fraction of exchangeable Sr taken up by plants (f =1), the thickness attributed to "surface horizons" and "deep horizons" was empirically determined. For shrubs (B. nana, V. vitis-idaea), the foliar <sup>87</sup>Sr/<sup>86</sup>Sr ratios can be explained with surface and deep horizons set at 0–5 cm and 5–40 cm, respectively (Table A.5). Even if this is in line with the maximum rooting depth measured for these shrub species at the study site (up to 35 cm for B. nana, and 40 cm for V. vitis-idaea; Fig. 5a; Hewitt et al 2018), this is deeper than the range of maximum rooting depth reported for these shrub species at the Arctic scale (~3-30 cm, B. nana; 5-10 cm, V. vitis-idaea; Iversen et al., 2015), especially for V. vitis-idaea. This highlights the importance to consider the variability of base cation sources with soil depth even for shallowly-rooted plant species. For the sedge (E. vaginatum), the foliar <sup>87</sup>Sr/<sup>86</sup>Sr ratios can be explained with surface and deep horizons set at 0-40 cm and 40-60 cm, respectively (Table A.5). This demonstrates that the sedge requires base cation sources up to 60 cm, which is deeper than the maximum rooting depth reported for this plant species at the site (~30-40 cm; Hewitt et al., 2018) and reported in the Arctic (~35-40 cm; Iversen et al., 2015). This could be explained by the capacity of *E. vaginatum* to explore deeper soil volumes, as demonstrated experimentally (Blume-Werry et al., 2019; Keuper et al., 2017). This adds to the importance of considering the variability of base cation sources with soil depth.

The quantitative isotope mass balance based on foliar  $^{87}$ Sr/ $^{86}$ Sr ratios supports changes in the contribution from deeper horizons as base cation sources for the three plant species between poorly and highly thawed sites. More specifically, the quantitative mass balance supports that *V. vitis-idaea* takes up  $31 \pm 21$ % of Sr below 5 cm, i.e., from 26 % on poorly thawed soil profiles (Min1, Min3, Mod1, Ext1) to 40 % on highly thawed soil profiles (Mod2, Mod3, Ext3) (Table A.5). Considering the rooting depth of *V. vitis-idaea*, the main difference between poorly thawed and highly thawed soil profiles below 5 cm is the thickness of the organic layer changing from 40 to 20 cm (Fig. 5b) and the associated increase in base saturation (ratio of the sum of exchangeable Ca, K, Mg, Na over the soil cation exchange capacity) between  $\sim 20$  and 40 cm driven by the mineral active layer (Fig. 5c). This increase in base saturation is driven by the increase in the total reserve in bases in the mineral active layer relative to the organic active layer (Fig. 5d). The changing

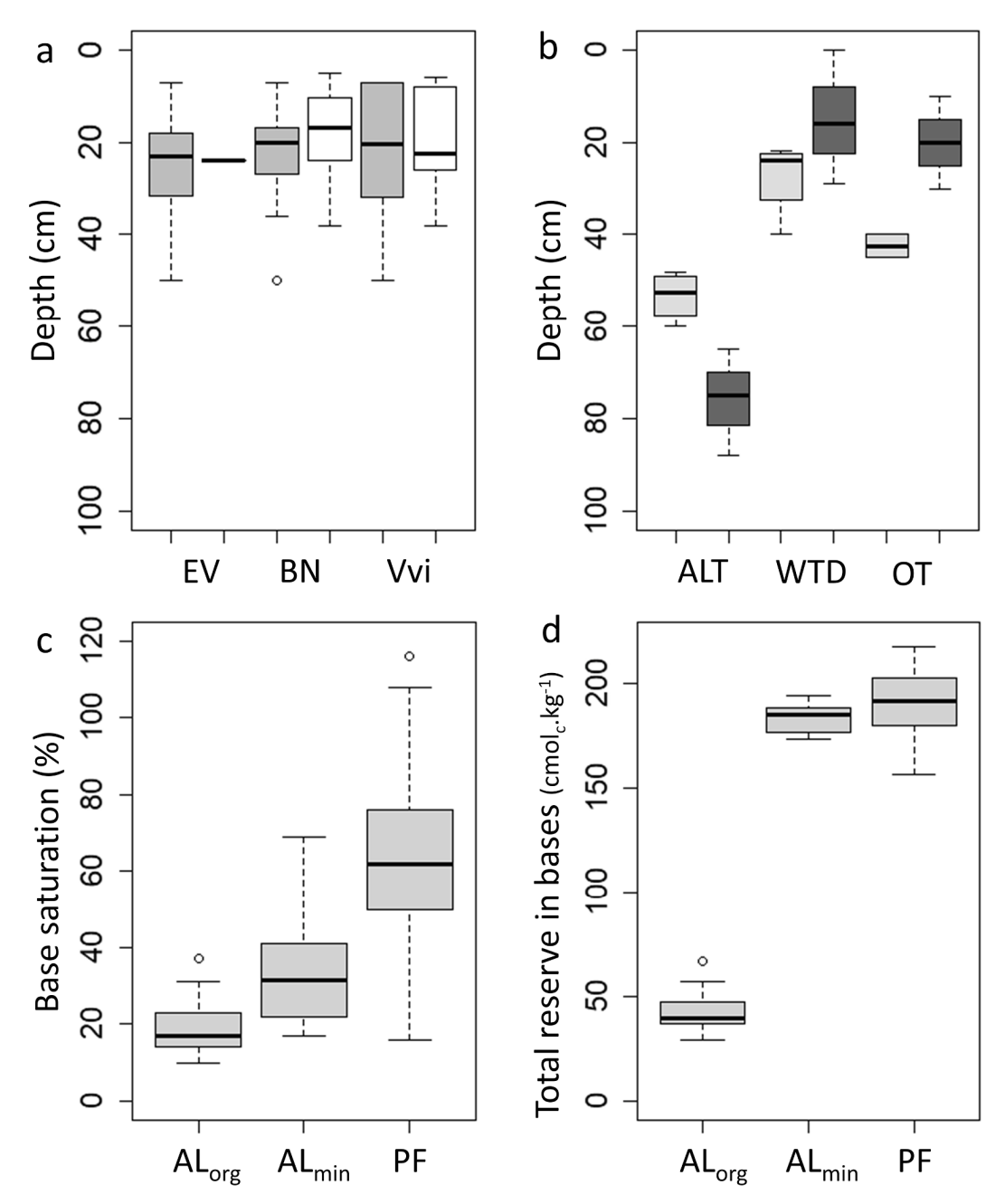


Fig. 5. (a) Maximum rooting depth of *E. vaginatum* (EV), *B. nana* (BN) and *V. vitis-idaea* (Vvi) at the site of Eight Mile Lake in patches of sedge-dominated tundra (<25% cover as shrubs; grey) and shrub-dominated tundra (25-75% cover as shrubs; white) (data from Hewitt et al 2018). (b) Mesured active layer thickness (ALT), water table depth (WTD) and organic-mineral transition (OT) for the four poorly thawed (light grey) and the three highly thawed (dark grey) soil profiles (data in Table A.5). (c) Base saturation (ratio of the sum of exchangeable Ca, K, Mg, Na over the soil cation exchange capacity) in organic ( $AL_{org}$ ) and mineral ( $AL_{min}$ ) active layer (>and < 20 % of organic C content for  $AL_{org}$  and  $AL_{min}$ , respectively), and in permafrost (PF) for the seven soil profiles of this study (data from (Mauclet et al., 2022b). (d) Total Reserve in Bases (TRB, sum of total concentrations in Ca, K, Mg, Na expressed in cmolc.kg $^{-1}$ ) in organic ( $AL_{org}$ ) and mineral ( $AL_{min}$ ) active layer (>and < 20 % of organic C content for  $AL_{org}$  and  $AL_{min}$ , respectively), and in permafrost (PF) (data in Table A.2). (Figure in color).

foliar  $^{87}$ Sr/ $^{86}$ Sr ratios of *V. vitis-idaea* towards lower values between poorly and highly thawed soil profiles support that thawing conditions provide a more readily available source of base cations for plant uptake below 5 cm than between 0 and 5 cm. The same applies for *B. nana* which takes up 65  $\pm$  26 % of Sr below 5 cm, i.e., from 60 % on poorly thawed soil profiles up to 75 % on highly thawed soil profiles (Table A.5).

The quantitative mass balance shows that *E. vaginatum* takes up  $35\pm29$  % of Sr from deeper layers below 40 cm on poorly thawed profiles, i. e., with a mean value decreasing from 45 % on poorly thawed profiles to 22 % on highly thawed profiles (Table A.5). The decrease is especially

driven by minimal contribution from layers below 40 cm for the two profiles with the thinnest organic layer (10 and 20 cm for Mod2 and Mod3, respectively; Table A.1). These data can be explained by the fact that a thinner organic layer is associated with an increase in base saturation in the 0–40 cm layer (Fig. 5b and c), which is directly available for the roots. This observation is fully in line with the explanation provided for the change in foliar <sup>87</sup>Sr/<sup>86</sup>Sr ratios of *V. vitis-idaea* and *B. nana* between poorly and highly thawed soil profiles.

The foliar <sup>87</sup>Sr/<sup>86</sup>Sr data of the three plant species studied support that micro-landscape variability of the exchangeable base cation reserve in the soil are key to consider in the context of permafrost thaw, i.e., a

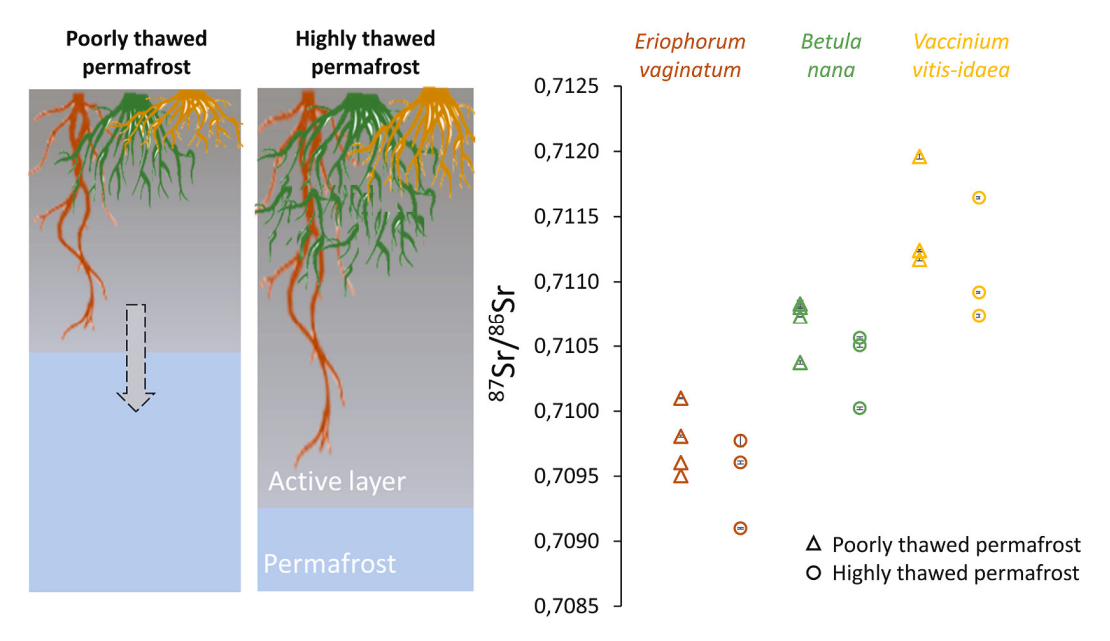


Fig. 6. Radiogenic Sr isotopic signature in foliar tissues of three dominant Arctic tundra plant species: *E. vaginatum, B. nana*, and *V. vitis-idaea*, upon poorly and highly thawed permafrost conditions (Eight Mile Lake, Alaska, USA). Error bars for isotopic measurements are smaller than the data points. (Figure in color).

source of readily available nutrients both for shallow- and deep-rooted plant species. This highlights that in addition to the release of nutrients at the thaw front more reachable by deep-rooted plants (Blume-Werry et al., 2019; Salmon et al., 2016; Wang et al., 2016), changes in mineral nutrient reserve with depth in the root zone across the landscape are to be accounted for to better understand the controls on the ongoing shift in Arctic tundra vegetation. This shift may depend on the balance between the benefits associated with deeper root distribution (sedges benefitting first from permafrost thaw), and earlier root growth (shallow-rooted shrubs taking advantage of the nutrient pulse after snowmelt in the early growing season; Wang et al., 2016). Future perspectives should consider the influence on the sedge and shrub species development of increasing subsidence upon permafrost thaw (Rodenhizer et al., 2020) which likely enhances the micro-landscape variability of the mineral nutrient reserve and the distribution of the pool of exchangeable base cations.

## 5. Conclusions

In this study, we determined the influence of permafrost degradation on the base cation sources for Arctic tundra vegetation (*B. nana, V. vitisidaea*, and *E. vaginatum*) by using the radiogenic Sr isotope ratio as a tracer of source along a permafrost thaw gradient at Eight Mile Lake, Interior Alaska, USA. The main following conclusions can be drawn:

- (i) The more radiogenic foliar <sup>87</sup>Sr/<sup>86</sup>Sr ratios of shallow-rooted Arctic tundra shrubs (*B. nana, V. vitis-idaea*) reflect a shallow source of soil exchangeable Sr from surface soil horizons, whereas the less radiogenic foliar <sup>87</sup>Sr/<sup>86</sup>Sr ratios of deep-rooted Arctic tundra sedges (*E. vaginatum*) reflect a source of Sr from deeper soil horizons.
- (ii) The change towards less radiogenic foliar <sup>87</sup>Sr/<sup>86</sup>Sr ratio in the three plant species between poorly and highly thawed soil profiles supports that micro-landscape variability of the exchangeable base cation reserve with soil depth is a key source of readily available nutrients both for shallow- and deep-rooted plant species upon permafrost thaw.
- (iii) The data support that changing nutrient sources upon permafrost thaw is not restricted to the deep-rooted species closer to the permafrost thaw front. With permafrost thaw, changes in mineral nutrient reserve with depth in the root zone should be considered.

Overall, this study contributes to support that upon permafrost thaw,

differences in plant strategies for nutrient uptake may largely influence the interactions between deep- and shallow-rooted plant species. This is beyond the common view that nutrient release at the permafrost thaw front preferentially benefits deep-rooted plant species.

## **Declaration of Competing Interest**

The authors declare that they have no known competing financial interests or personal relationships that could have appeared to influence the work reported in this paper.

## Data availability

All data are made available (in the appendix or as a link to a database with a doi provided).

# Acknowledgements

We thank S. Malvaux, M. Thomas, S. François and the WeThaw team at UCLouvain for valuable scientific exchanges and help in the field. We warmly acknowledge the MOCA analytical platform at UCLouvain for the mineral elemental analyses: A. Iserentant, C. Givron, L. Monin, and E. Devos. We also greatly thank J. Ledman and the Schuur Lab (Northern Arizona University) for their scientific support and their help with site selection. We acknowledge the associate editor Alberto Agnelli and two anonymous reviewers for their constructive comments.

# Funding

This work was supported by the European Union's Horizon 2020 research and innovation program (grant agreement No. 714617, 2017-2022) and by the Fund for Scientific Research FNRS in Belgium to SO (FC69480).

# Appendix A. Supplementary data

Supplementary data to this article can be found online at https://doi.org/10.1016/j.geoderma.2022.116277.

#### References

- Åberg, G., Jacks, G., Joseph Hamilton, P., 1989. Weathering rates and 87Sr/86Sr ratios: an isotopic approach. J Hydrol. 109, 65–78. https://doi.org/10.1016/0022-1694 (89)90007-3.
- Aciego, S.M., Bourdon, B., Lupker, M., Rickli, J., 2009. A new procedure for separating and measuring radiogenic isotopes (U, Th, Pa, Ra, Sr, Nd, Hf) in ice cores. Chem. Geol. 266, 194–204. https://doi.org/10.1016/j.chemgeo.2009.06.003.
- Anderson, J., Lévesque, N., Caron, F., Beckett, P., Spiers, G.A., 2022. A review on the use of lichens as a biomonitoring tool for environmental radioactivity. J. Environ. Radioact. 243, 106797 https://doi.org/10.1016/j.jenvrad.2021.106797.
- Bataille, C.P., Crowley, B.E., Wooller, M.J., Bowen, G.J., 2020. Advances in global bioavailable strontium isoscapes. Palaeogeogr. Palaeoclimatol. Palaeoecol. 555, 109849 https://doi.org/10.1016/j.palaeo.2020.109849.
- Blum, J.D., Taliaferro, E.H., Weisse, M.T., Holmes, R.T., 2000. Changes in Sr/Ca, Ba/Ca and 87Sr/86Sr ratios between trophic levels in two forest ecosystems in the northeastern U.S.A. Biogeochemistry 49, 87–101. https://doi.org/10.1023/A: 1006390707989.
- Blume-Werry, G., Milbau, A., Teuber, L.M., Johansson, M., Dorrepaal, E., 2019. Dwelling in the deep – strongly increased root growth and rooting depth enhance plant interactions with thawing permafrost soil. New Phytol. 223, 1328–1339. https://doi. org/10.1111/pph.15903.
- Bracho, R., Natali, S., Pegoraro, E., Crummer, K.G., Schädel, C., Celis, G., Hale, L., Wu, L., Yin, H., Tiedje, J.M., Konstantinidis, K.T., Luo, Y., Zhou, J., Schuur, E.A.G., 2016. Temperature sensitivity of organic matter decomposition of permafrost-region soils during laboratory incubations. Soil Biol. Biochem. 97, 1–14. https://doi.org/10.1016/i.soilbio.2016.02.008.
- Bullen, T., Chadwick, O., 2016. Ca, Sr and Ba stable isotopes reveal the fate of soil nutrients along a tropical climosequence in Hawaii. Chem. Geol. 422, 25–45. https://doi.org/10.1016/j.chemgeo.2015.12.008.
- Capo, R.C., Stewart, B.W., Chadwick, O.A., 1998. Strontium isotopes as tracers of ecosystem processes: theory and methods. Geoderma 82, 197–225. https://doi.org/ 10.1016/S0016-7061(97)00102-X.
- Celis, G., Ledman, J., Bracho, R., Schuur, E.A.G., 2019. Eight Mile Lake Research Watershed, Thaw Gradient: half-hourly soil temperature 2004-2018, Bonanza Creek LTER - University of Alaska Fairbanks. BNZ:517. https://doi.org/doi:10.6073/pasta/ 29d79cf984929bc247173268c3785eca.
- Chadwick, O.A., Derry, L.A., Vitousek, P.M., Huebert, B.J., Hedin, L.O., 1999. Changing sources of nutrients during four million years of ecosystem development. Nature 397, 491–497. https://doi.org/10.1038/17276.
- Chadwick, O.A., Derry, L.A., Bern, C.R., Vitousek, P.M., 2009. Changing sources of strontium to soils and ecosystems across the Hawaiian Islands. Chem. Geol. 267, 64–76. https://doi.org/10.1016/j.chemgeo.2009.01.009.
- Chao, T.T., Sanzolone, R.F., 1992. Decomposition techniques. J. Geochem. Explor. Geoanalysis 44, 65–106. https://doi.org/10.1016/0375-6742(92)90048-D.
- Chapin, F.S., Sturm, M., Serreze, M.C., Mcfadden, J.P., Key, J.R., Lloyd, A.H., McGuire, A.D., Rupp, T.S., Lynch, A.H., Schimel, J.P., Chapman, W.L., Epstein, H.E., Euskirchen, E.S., Hinzman, L.D., Jia, G., Ping, C.L., Tape, K.D., Thompson, C.D.C., Walker, D.A., Welker, J.M., 2005. Role of land-surface changes in Arctic summer warming. Science 310, 657–660. https://doi.org/10.1126/science.1117368.
- Cornelis, J.-T., Delvaux, B., Cardinal, D., André, L., Ranger, J., Opfergelt, S., 2010. Tracing mechanisms controlling the release of dissolved silicon in forest soil solutions using Si isotopes and Ge/Si ratios. Geochim. Cosmochim. Acta 74, 3913–3924. https://doi.org/10.1016/j.gca.2010.04.056.
- DalCorso, G., Manara, A., Piasentin, S., Furini, A., 2014. Nutrient metal elements in plants. Metallomics 6, 1770–1788. https://doi.org/10.1039/c4mt00173g.
- Deane-Coe, K.K., Mauritz, M., Celis, G., Salmon, V., Crummer, K.G., Natali, S.M., Schuur, E.A.G., 2015. Experimental warming alters productivity and isotopic signatures of tundra mosses. Ecosystems 18, 1070–1082. https://doi.org/10.1007/ s10021-015-9884-7.
- Derry, L.A., Chadwick, O.A., 2007. Contributions from earth's atmosphere to soil. Elements 3, 333–338. https://doi.org/10.2113/gselements.3.5.333.
- Drouet, T.h., Herbauts, J., Gruber, W., Demaiffe, D., 2005. Strontium isotope composition as a tracer of calcium sources in two forest ecosystems in Belgium. Geoderma 126, 203–223. https://doi.org/10.1016/j.geoderma.2004.09.010.
- Drouet, T.h., Herbauts, J., Gruber, W., Demaiffe, D., 2007. Natural strontium isotope composition as a tracer of weathering patterns and of exchangeable calcium sources in acid leached soils developed on loess of central Belgium. Eur. J. Soil Sci. 58, 302–319. https://doi.org/10.1111/j.1365-2389.2006.00840.x.
- Goldich, S.S., 1938. A study in rock-weathering. J. Geol. 46, 17–58. https://doi.org/ 10.1086/624619.
- Graustein, W.C., Armstrong, R.L., 1983. The use of strontium-87/strontium-86 ratios to measure atmospheric transport into forested watersheds. Science 219, 289–292. https://doi.org/10.1126/science.219.4582.289.
- Hajj, F., Poszwa, A., Bouchez, J., Guérold, F., 2017. Radiogenic and "stable" strontium isotopes in provenance studies: a review and first results on archaeological wood from shipwrecks. J. Archaeol. Sci. 86, 24–49. https://doi.org/10.1016/j.iss.2017.09.005
- Herbillon, A.J., 1986. Chemical estimation of weatherable minerals present in the diagnostic horizons of low activity clay soils. Presented at the Proceedings of the 8th international soil classification workshop: classification, characterization and utilization of oxisols, RJ. Proceeding, Rio de Janeiro, pp. 39–48.
- Hewitt, R.E., Taylor, D.L., Genet, H., McGuire, A.D., Mack, M.C., 2018. Below-ground plant traits influence tundra plant acquisition of newly thawed permafrost nitrogen. J. Ecol. 107, 950–962. https://doi.org/10.1111/1365-2745.13062.

Hicks Pries, C.E., Schuur, E.A.G., Crummer, K.G., 2012. Holocene carbon stocks and carbon accumulation rates altered in soils undergoing permafrost thaw. Ecosystems 15, 162–173. https://doi.org/10.1007/s10021-011-9500-4.

- Hirst, C., Mauclet, E., Monhonval, A., Tihon, E., Ledman, J., Schuur, E.A.G., Opfergelt, S., 2022. Seasonal changes in hydrology and permafrost degradation control mineral element-bound DOC transport from permafrost soils to streams. Global Biogeochem. Cycles. https://doi.org/10.1029/2021GB007105.
- Hutchings, J.A., Bianchi, T.S., Kaufman, D.S., Kholodov, A.L., Vaughn, D.R., Schuur, E.A. G., 2019. Millennial-scale carbon accumulation and molecular transformation in a permafrost core from Interior Alaska. Geochim. Cosmochim. Acta 253, 231–248. https://doi.org/10.1016/j.gca.2019.03.028.
- IUSS Working Group WRB, 2015. World Reference Base for Soil Resources 2014, update 2015 International soil classification system for naming soils and creating legends for soil maps. World Soil Resources Reports, FAO, Rome.
- Iversen, C.M., Sloan, V.L., Sullivan, P.F., Euskirchen, E.S., McGuire, A.D., Norby, R.J., Walker, A.P., Warren, J.M., Wullschleger, S.D., 2015. The unseen iceberg: plant roots in arctic tundra. New Phytol. 205, 34–58. https://doi.org/10.1111/nph.13003.
- Jasinski, B., Schuur, E.A.G., Mack, M.C., 2018. Eight Mile Lake Research Watershed, Thaw Gradient: peak growing season aboveground biomass 2017. Bonanza Creek LTEP
- Jasinski, B., Hewitt, R.E., Mauritz, M., Miller, S.N., Schuur, E.A.G., Taylor, M.A., Walker, X.J., Mack, M.C., 2022. Plant foliar nutrient response to active layer and water table depth in warming permafrost soils. J. Ecol. 1365–2745, 13864. https://doi.org/10.1111/1365-2745.13864.
- Jonsdottir, I.S., Magnusson, B., Gudmundsson, J., Elmarsdottir, A., Hjartarson, H., 2005. Variable sensitivity of plant communities in Iceland to experimental warming. Global Change Biol. 11, 553–563. https://doi.org/10.1111/j.1365-2486.2005.00928.x.
- Jorgenson, M.T., Racine, C.H., Walters, J.C., Osterkamp, T.E., 2001. Permafrost degradation and ecological changes associated with a warming climate in Central Alaska. Clim. Change 551–579. https://doi.org/10.1023/A:1005667424292.
- Jorgenson, J.C., Raynolds, M.K., Reynolds, J.H., Benson, A.-M., 2015. Twenty-five year record of changes in plant cover on tundra of Northeastern Alaska. Arct. Antarct. Alp. Res. 47, 785–806. https://doi.org/10.1657/AAAR0014-097.
- Jorgenson, M.T., Shur, Y.L., Pullman, E.R., 2006. Abrupt increase in permafrost degradation in Arctic Alaska. Geophys. Res. Lett. 33, L02503. https://doi.org/ 10.1029/2005GL024960.
- Karlsson, P.S., 1985. Effects of water and mineral nutrient supply on a deciduous and an evergreen dwarf shrub: Vaccinium uliginosum L. and V. vitisidaea L. Ecography 8, 1–8. https://doi.org/10.1111/j.1600-0587.1985.tb01146.x.
- Keller, K., Blum, J.D., Kling, G.W., 2007. Geochemistry of soils and streams on surfaces of varying ages in Arctic Alaska. aare 39, 84–98. https://doi.org/10.1657/1523-0430 (2007)39[84:GOSASO]2.0.CO;2.
- Kennedy, M.J., Chadwick, O.A., Vitousek, P.M., Derry, L.A., Hendricks, D.M., 1998. Changing sources of base cations during ecosystem development, Hawaiian Islands. Geology 26, 1015–1018. https://doi.org/10.1130/00091-7613(1998)026<1015: CSOBCD>2.3.CO:2.
- Keuper, F., Dorrepaal, E., van Bodegom, P.M., van Logtestijn, R., Venhuizen, G., van Hal, J., Aerts, R., 2017. Experimentally increased nutrient availability at the permafrost thaw front selectively enhances biomass production of deep-rooting subarctic peatland species. Glob. Chang. Biol. 23, 4257–4266. https://doi.org/ 10.1111/cpcb.13804
- Koch, J.C., Runkel, R.L., Striegl, R., McKnight, D.M., 2013. Hydrologic controls on the transport and cycling of carbon and nitrogen in a boreal catchment underlain by continuous permafrost. J. Geophys. Res. Biogeosci. 118, 698–712. https://doi.org/ 10.1002/jgrg.20058.
- Kwon, M.J., Natali, S.M., Hicks Pries, C.E., Schuur, E.A.G., Steinhof, A., Crummer, K.G., Zimov, N., Zimov, S.A., Heimann, M., Kolle, O., Göckede, M., 2019. Drainage enhances modern soil carbon contribution but reduces old soil carbon contribution to ecosystem respiration in tundra ecosystems. Glob. Change Biol. 25, 1315–1325. https://doi.org/10.1111/gcb.14578.
- Lewis, K.C., Zyvoloski, G.A., Travis, B., Wilson, C., Rowland, J., 2012. Drainage subsidence associated with Arctic permafrost degradation. J. Geophys. Res. 117, n/an/a. https://doi.org/10.1029/2011JF002284.
- Lloyd, A.H., Yoshikawa, K., Fastie, C.L., Hinzman, L., Fraver, M., 2003. Effects of permafrost degradation on woody vegetation at arctic treeline on the Seward Peninsula, Alaska. Permafrost Periglac. Process. 14, 93–101. https://doi.org/ 10.1002/ppp.446.
- Mauclet, E., Agnan, Y., Hirst, C., Monhonval, A., Pereira, B., Vandeuren, A., Villani, M., Ledman, J., Taylor, M., Jasinski, B.L., Schuur, E.A.G., Opfergelt, S., 2022a. Changing sub-Arctic tundra vegetation upon permafrost degradation: impact on foliar mineral element cycling. Biogeosciences 19, 2333–2351. https://doi.org/10.5194/bg-19-2333-2022
- Mauclet, E., Villani, M., Monhonval, A., Hirst, C., Schuur, E.A.G., Opfergelt, S., 2022b. Characterization of permafrost soil exchange properties and quantification of stocks in soil exchangeable base cations. Open Data @ UCLouvain. https://doi.org/10.14428/DVN/FQVMEP.
- Metson, A.J., 1956. Methods of Chemical Analysis for Soil Survey Samples. New Zealand Soil Bureau Bulletin. D.S.I.R, Wellington, N.Z.
- Monhonval, A., Mauclet, E., Pereira, B., Vandeuren, A., Strauss, J., Grosse, G., Schirrmeister, L., Fuchs, M., Kuhry, P., Opfergelt, S., 2021. Mineral element stocks in the yedoma domain: a novel method applied to ice-rich permafrost regions. Front. Earth Sci. 9, 703304 https://doi.org/10.3389/feart.2021.703304.
- Naeth, M.A., Wilkinson, S.R., 2008. Lichens as biomonitors of air quality around a diamond mine, Northwest Territories, Canada. J. Environ. Qual. 37, 1675–1684. https://doi.org/10.2134/jeq2007.0090.

- Natali, S.M., Schuur, E.A.G., Trucco, C., Hicks Pries, C.E., Crummer, K.G., Baron Lopez, A.F., 2011. Effects of experimental warming of air, soil and permafrost on carbon balance in Alaskan tundra. Glob. Chang. Biol. 17, 1394–1407. https://doi.org/10.1111/j.1365-2486.2010.02303.x.
- Natali, S.M., Schuur, E.A.G., Rubin, R.L., 2012. Increased plant productivity in Alaskan tundra as a result of experimental warming of soil and permafrost. J. Ecol. 100, 488–498. https://doi.org/10.1111/j.1365-2745.2011.01925.x.
- Osterkamp, T.E., Romanovsky, V.E., 1999. Evidence for warming and thawing of discontinuous permafrost in Alaska 21. https://doi.org/10.1002/(SICI)1099-1530 (199901/03)10:1<17::AID-PPP303>3.0.CO;2-4.
- Osterkamp, T.E., Jorgenson, M.T., Schuur, E.a.G., Shur, Y.L., Kanevskiy, M.Z., Vogel, J. G., Tumskoy, V.E., 2009. Physical and ecological changes associated with warming permafrost and thermokarst in Interior Alaska. Permafr. Periglac. Process. 20, 235–256. https://doi.org/10.1002/ppp.656.
- Palmtag, J., Hugelius, G., Lashchinskiy, N., Tamstorf, M.P., Richter, A., Elberling, B., Kuhry, P., 2015. Storage, landscape distribution, and burial history of soil organic matter in contrasting areas of continuous permafrost. Arct. Antarct. Alp. Res. 47, 71–88. https://doi.org/10.1657/AAAR0014-027.
- Pearce, C.R., Parkinson, I.J., Gaillardet, J., Charlier, B.L.A., Mokadem, F., Burton, K.W., 2015. Reassessing the stable (888/86Sr) and radiogenic (87Sr/86Sr) strontium isotopic composition of marine inputs. Geochim. Cosmochim. Acta 157, 125–146. https://doi.org/10.1016/j.gca.2015.02.029.
- Pearson, R.G., Phillips, S.J., Loranty, M.M., Beck, P.S.A., Damoulas, T., Knight, S.J., Goetz, S.J., 2013. Shifts in Arctic vegetation and associated feedbacks under climate change. Nat. Clim. Change 3, 673-677. https://doi.org/10.1038/nclimate1858.
- Peech, M., 1965. Hydrogen-Ion Activity, in: Norman, A.G. (Ed.), Agronomy Monographs. American Society of Agronomy, Soil Science Society of America, Madison, WI, USA, pp. 914–926. https://doi.org/10.2134/agronmonogr9.2.c9.
- Pett-Ridge, J.C., Derry, L.A., Kurtz, A.C., 2009. Sr isotopes as a tracer of weathering processes and dust inputs in a tropical granitoid watershed, Luquillo Mountains, Puerto Rico. Geochim. Cosmochim. Acta 73, 25–43. https://doi.org/10.1016/j. gca.2008.09.032.
- Post, E., Alley, R.B., Christensen, T.R., Macias-Fauria, M., Forbes, B.C., Gooseff, M.N., Iler, A., Kerby, J.T., Laidre, K.L., Mann, M.E., Olofsson, J., Stroeve, J.C., Ulmer, F., Virginia, R.A., Wang, M., 2019. The polar regions in a 2°C warmer world. Sci. Adv. 5, eaaw9883. https://doi.org/10.1126/sciadv.aaw9883.
- Poszwa, A., Ferry, B., Dambrine, E., Pollier, B., Wickman, T., Loubet, M., Bishop, K., 2004. Variations of bioavailable Sr concentration and <sup>87</sup> Sr/ <sup>86</sup> Sr ratio in boreal forest ecosystems. Biogeochemistry 67, 1–20. https://doi.org/10.1023/B: BIOG.0000015162.12857.3e.
- Probst, A., El Gh'mari, A., Aubert, D., Fritz, B., McNutt, R., 2000. Strontium as a tracer of weathering processes in a silicate catchment polluted by acid atmospheric inputs, Strengbach, France. Chem. Geol. 170, 203–219. https://doi.org/10.1016/S0009-2541(99)00248-X.
- R Core Team, 2019. R: A Language and Environment for Statistical Computing. Austria, Vienna.
- Reimann, C., Filzmoser, P., Garrett, R.G., Dutter, R., 2008. Statistical Data Analysis Explained. https://doi.org/10.1002/9780470987605.
- Reynolds, A.C., Quade, J., Betancourt, J.L., 2012. Strontium isotopes and nutrient sourcing in a semi-arid woodland. Geoderma 189–190, 574–584. https://doi.org/ 10.1016/j.seoderma.2012.06.029.
- Rodenhizer, H., Ledman, J., Mauritz, M., Natali, S.M., Pegoraro, E., Plaza, C., Romano, E., Schädel, C., Taylor, M., Schuur, E., 2020. Carbon thaw rate doubles when accounting for subsidence in a permafrost warming experiment. J. Geophys. Res. Biogeosci. 125 https://doi.org/10.1029/2019JG005528.
- Salmon, V.G., Soucy, P., Mauritz, M., Celis, G., Natali, S.M., Mack, M.C., Schuur, E.A.G., 2016. Nitrogen availability increases in a tundra ecosystem during five years of experimental permafrost thaw. Glob. Change Biol. 22, 1927–1941. https://doi.org/ 10.1111/gcb.13204.
- Schuur, E.A.G., Crummer, K.G., Vogel, J.G., Mack, M.C., 2007. Plant species composition and productivity following permafrost thaw and thermokarst in Alaskan tundra. Ecosystems 10, 280–292. https://doi.org/10.1007/s10021-007-9024-0.
- Schuur, E.A.G., Bracho, R., Celis, G., Belshe, E.F., Ebert, C., Ledman, J., Mauritz, M., Pegoraro, E.F., Plaza, C., Rodenhizer, H., Romanovsky, V., Schädel, C., Schirokauer, D., Taylor, M., Vogel, J.G., Webb, E.E., 2021. Tundra underlain by

- thawing permafrost persistently emits carbon to the atmosphere over 15 years of measurements. J. Geophys. Res. Biogeosci. 126 https://doi.org/10.1029/
- Schuur, E.A.G., Mack, M.C., 2018. Ecological response to permafrost thaw and consequences for local and global ecosystem services. Annu. Rev. Ecol. Evol. Syst. 49, 279–301. https://doi.org/10.1146/annurev-ecolsys-121415-032349.
- Schuur, E.A.G., Vogel, J.G., Crummer, K.G., Lee, H., Sickman, J.O., Osterkamp, T.E., 2009. The effect of permafrost thaw on old carbon release and net carbon exchange from tundra. Nature 459, 556–559. https://doi.org/10.1038/nature08031.
- Shaver, G.R., Bret-Harte, M.S., Jones, M.H., Johnstone, J., Gough, L., Laundre, J., Chapin, F.S., 2001. Species composition interacts with fertilizer to control long-term change in tundra productivity. Ecology 82, 3163–3181. https://doi.org/10.1890/ 0012-9658(2001)082[3163:SCIWFTI2.0.CO:2.
- Stevenson, E.I., Aciego, S.M., Chutcharavan, P., Parkinson, I.J., Burton, K.W., Blakowski, M.A., Arendt, C.A., 2016. Insights into combined radiogenic and stable strontium isotopes as tracers for weathering processes in subglacial environments. Chem. Geol. 429, 33–43. https://doi.org/10.1016/j.chemgeo.2016.03.008.
- Sturm, M., Mcfadden, J.P., Liston, G.E., Chapin, F.S., Racine, C.H., Holmgren, J., 2001a. Snow–shrub interactions in Arctic tundra: a hypothesis with climatic implications. J. Clim. 14, 9.
- Sturm, M., Racine, C., Tape, K., 2001b. Increasing shrub abundance in the Arctic. Nature 411, 546–547. https://doi.org/10.1038/35079180.
- Tetzlaff, D., Buttle, J., Carey, S.K., McGuire, K., Laudon, H., Soulsby, C., 2015. Tracer-based assessment of flow paths, storage and runoff generation in northern catchments: a review. Hydrol. Process. 29, 3475–3490. https://doi.org/10.1002/hyp.10412.
- van der Kolk, H.-J., Heijmans, M.M.P.D., van Huissteden, J., Pullens, J.W.M., Berendse, F., 2016. Potential Arctic tundra vegetation shifts in response to changing temperature, precipitation and permafrost thaw. Biogeosciences 13, 6229–6245. https://doi.org/10.5194/bg-13-6229-2016.
- Villani, M., Mauclet, E., Agnan, Y., Druel, A., Jasinski, B., Taylor, M., Schuur, E.A.G., Opfergelt, S., 2022. Mineral element recycling in topsoil following permafrost degradation and a vegetation shift in sub-Arctic tundra. Geoderma 421, 115915. https://doi.org/10.1016/j.geoderma.2022.115915.
- Vitousek, P.M., 2004. Nutrient Cycling and Limitation: Hawai'i as a Model System, Princeton Environmental Institute Series. Princeton University Press, Princeton, NJ.
- Vitousek, P.M., Kennedy, M.J., Derry, L.A., Chadwick, O.A., 1999. Weathering versus atmospheric sources of strontium in ecosystems on young volcanic soils. Oecologia 121, 255–259. https://doi.org/10.1007/s004420050927.
- Vogel, J., Schuur, E.A.G., Trucco, C., Lee, H., 2009. Response of CO<sub>2</sub> exchange in a tussock tundra ecosystem to permafrost thaw and thermokarst development.
  J. Geophys. Res. Biogeo. 114 https://doi.org/10.1029/2008JG000901.
- Walker, D.A., Raynolds, M.K., Daniëls, F.J.A., Einarsson, E., Elvebakk, A., Gould, W.A., Katenin, A.E., Kholod, S.S., Markon, C.J., Melnikov, E.S., Moskalenko, N.G., Talbot, S.S., Yurtsev, B.A.(†), The other members of the CAVM Team, 2005. The Circumpolar Arctic vegetation map. Journal of Vegetation Science 16, 267–282. https://doi.org/10.1111/j.1654-1103.2005.tb02365.x.
- Walvoord, M.A., Kurylyk, B.L., 2016. Hydrologic impacts of thawing permafrost—A review. Vadose Zone J. 15 https://doi.org/10.2136/vzj2016.01.0010.
- Wang, P., Mommer, L., van Ruijven, J., Berendse, F., Maximov, T.C., Heijmans, M.M.P. D., 2016. Seasonal changes and vertical distribution of root standing biomass of graminoids and shrubs at a Siberian tundra site. Plant Soil 407, 55–65. https://doi.org/10.1007/s11104-016-2858-5.
- Wang, X., Tang, Z., 2020. The first large-scale bioavailable Sr isotope map of China and its implication for provenance studies. Earth Sci. Rev. 210, 103353 https://doi.org/ 10.1016/j.earscirev.2020.103353.
- Wilson, F.H., Labay, K.A., 1997. Data compilation for USGS reference material BHVO-2, Hawaiian Basalt. US Geol. Surv. Open-File Rep. 1.
- Yang, M., Nelson, F.E., Shiklomanov, N.I., Guo, D., Wan, G., 2010. Permafrost degradation and its environmental effects on the Tibetan Plateau: a review of recent research. Earth Sci. Rev. 103, 31–44. https://doi.org/10.1016/j. earscirev.2010.07.002.
- Yoshikawa, K., Hinzman, L.D., 2003. Shrinking thermokarst ponds and groundwater dynamics in discontinuous permafrost near council, Alaska. Permafrost Periglac. Process. 14, 151–160. https://doi.org/10.1002/ppp.451.